Swansea University
Prifysgol Abertawe

Cronfa
Setting Research Free

Cronfa - Swansea University Open Access Repository

_____

This is an author produced version of a paper published in :
Powder Technology

_____

Cronfa URL for this paper:
http://cronfa.swan.ac.uk/Record/cronfa26429

_____

Paper:

_____

Accepted Manuscript

The identification of an accurate simulation approach to predict the effect of operational parameters on the particle size distribution (PSD) of powders produced by an industrial close-coupled gas atomiser

J.S. Thompson, O. Hassan, S.A. Rolland, J. Sienz

The identification of an accurate simulation approach to predict the effect of operational parameters on the Particle Size Distribution (PSD) of powders produced by an industrial close-coupled gas atomiser

JS. Thompson[1], O. Hassan, SA. Rolland, J. Sienz

College of Engineering, Swansea University Bay Campus, Neath Port Talbot, UK, SA1 8QQ

LSN Diffusion Ltd.[2]

Abstract

Powder Metallurgy (PM) refers to a range of engineering techniques whereby net shape or near-net shape bodies are produced through the aggregation of a powder substrate. Specifically, the emergence of Additive Layer Manufacturing (ALM) is an exciting development in this field. However, the quality of any product produced by ALM is highly dependent upon the quality of the powder used. Gas atomisation is a specialised processing route in the PM field for the production of fine, spherical powders directly from a molten metal melt. The close-coupled gas atomisation process involves a melt stream being impacted by high velocity, under-expanded gas jets which initiate its break-up in two distinct phases; the second critical in determining the final particle size distribution (PSD) of the powder produced. However, fully understanding the mechanisms at work and exerting a high level of control over any produced powder is a challenge faced by the powder manufacturing industry; highlighted by the stringent requirements of the new ALM manufacturing technique.

Utilising Ansys Fluent v14.5 computational fluid dynamics (CFD) software, a 3D axi-symmetric simulation has been developed of a close-coupled atomising gas jet nozzle configuration utilised by a powder manufacturer. Through the two-way coupling of the CFD with a Discrete Particle Model (DPM) using the Euler-Lagrange approach, an assessment has been made of the effect of process parameters on the final PSD of the metal powders produced. The most appropriate model for the simulation of the secondary break-up phase has been identified from the Kelvin-Helmholtz (KH), Kelvin-Helmholtz Rayleigh-Transport (KHRT) and Taylor Analogy Break-up (TAB) models. Subsequently, the validated simulation approach has been used for the qualitative assessment

[1]Tel: +44(0)1792 606871; Email: jennifer.thompson@swansea.ac.uk
[2]Industrial collaborator, LSN Diffusion Ltd., Ammanford, Carmarthenshire, UK, SA18 3GY.

of the effect of altering the atomising nozzle geometry and process conditions on
the average size of powders produced i.e. finer or coarser. It was also established
that there is potential for the model to be used as a quantitative predictive tool
of powder size; useful for quality control especially when manufacturing powder
for use in ALM. However, further development and validation is required for
confirmation of this function.

1. Introduction

The potential emergence of Additive Layer Manufacturing (ALM) into the
mainstream of bespoke part production highlights the importance of manufac-
turing fine, spherical, metal powders that meet any pre-defined specifications.
⁵ Gas atomisation is a complex multi-physics process which involves a molten
metal stream passing through an atomising nozzle system, in which high ve-
locity jets of an inert atomising gas impinge upon the stream resulting in its
disintegration into fine droplets [1, 2, 3]. It is extensively used as an efficient
manufacturing method for high quality powders, as required for ALM produc-
¹⁰ tion. However, it is the consensus within both industry and research that the
management of a tightly controlled gas atomisation production process is some-
thing of a "black art".

Close-coupled gas atomisation involves the molten metal stream being de-
livered into the atomising gas via a ceramic melt delivery tube, and is the most
¹⁵ commonly utilised configuration by industry [4, 5]. Figure 1 provides a simpli-
fied schematic of the close-coupled configuration; it should be noted that the
length of the melt delivery tube is a critical parameter in the performance of
the atomiser, as has been shown by Mi et al[6]. The length by which the melt
delivery tube extends beyond the level of the atomising gas jet's entry is termed
²⁰ protrusion length, as labelled in the Figure 1.

Figure 1: The close-coupled gas atomiser configuration

The atomising gas jet can be classified as under-expanded; where, an issuing
jet's flow is dominated by a strong internal shock wave formed from reflections
of strong expansion waves that develop at the nozzle exit [7]. The subsequent
jet structure that is established consists of shear mixing layers, Prandtl-Meyer
²⁵ expansion fans and shock waves [8]. The repeating, reflecting pattern of which
form a shock-cell diamond structure. When the flow conditions are correct,
i.e. at high operating pressure, a normal shock wave is formed, also termed a
Mach disc and the jet is now highly under-expanded [3, 9, 10]. However, due
to the construction of the close-coupled gas atomisation head, the flow is not
³⁰ only that of an under-expanded jet. Additionally, a fluid dynamic problem with
similarities to the flow-field of the backward facing step forms [11]. In particular,

2

a subsonic circulating region develops, that is critical to the overall efficiency of the gas atomisation process [9].

The formation of the Mach disc at the end of the circulating region effectively
35 cuts it off from the surrounding flow, resulting in a "closed-wake" atomisation process [12]. A particular observation of the closed-wake condition is that the pressure at the melt delivery tube exit, termed the "aspiration pressure", drops dramatically [9, 13, 10, 14, 6]. Generally, a strong sub-ambient aspiration pressure provides an increased draw on the issuing melt, which results in stable
40 atomisation less likely to experience issues such as freeze-off [9, 13]. A significant amount of literature has been generated on the topic of open/closed-wake atomisation and the operating conditions/nozzle geometry that dictates them. Observations include: closed-wake conditions result in finer powders with a narrower standard deviation [9, 10]; shorter protrusion lengths cause wake closure
45 to occur more gradually and at a lower operating pressure [6]; and, when in closed-wake condition, increasing the protrusion length results in a stronger sub-ambient aspiration pressure [6].

In addition to a sub-ambient pressure at the melt nozzle exit, a radial pressure gradient along the melt exit is established from the centre (maximum pres-
50 sure) to the edge, which drives the melt in this direction [6]. This in turn establishes pre-filming of the melt i.e. it forms a hollow sheet of metal around the melt nozzle's exit, which allows for more efficient primary break-up [10]. It is reported that increasing the protrusion length results in a more uniform pressure at the melt nozzle's exit. Therefore, it is a trade-off when increasing
55 protrusion length, between a strong sub-ambient aspiration pressure to draw the melt and a radial pressure gradient to drive the melt to pre-filming [6].

In order to estimate the effect of process parameters on the subsequent PSD of powders produced from the gas atomisation process it is necessary to implement a model which is capable of approximating the physics of the melt
60 break-up. The gas atomisation break-up process can be considered in two distinct phases: a primary phase, where the melt is shredded into ligaments which break-down to form an ensemble of large droplets; with, a secondary phase taking place to further reduce the droplet size prior to solidification, which is critical in determining the final particle size distribution (PSD) of powders pro-
65 duced. Considering the melt break-up mechanisms, the main parameter related to break-up physics is the gas Weber number, We_g, defined as [11]:

$$We_g = \frac{\rho_g u_r^2 d_p}{\sigma} \tag{1}$$

where, σ is the surface tension of the droplet; ρ_g the density of the gas; d_p the particle/droplet's diameter and u_r is the relative velocity between gas and droplet. The We_g and whether it is low or high, dictates the physical mechanism
70 of secondary break-up. It provides the ratio of aerodynamic forces acting upon the droplet to the resistive forces of the droplet break-up, governed by surface tension. Low values of We_g, typically less than 80, result in the "bag break-up" process. This occurs when surface tension forces are high enough to result in an outward force forming an inflated balloon or bag shape, which breaks down

3

75 via perforation into a cloud of fine droplets [1, 15, 11]. At high We_g values, the forces turn inwards in the "ligament break-up regime", where ligaments are sheared from the outer part of the droplet, resulting in the formation of an octopus-like shape. The octopus arms then thin and break-up into smaller droplets [1]. Generally, it is found that the Taylor Analogy Break-up (TAB)

80 break-up model best represents bag break-up for a We_g in the range of 10 to 80; whilst, the Kelvin-Helmholtz (KH) or Kelvin-Helmholtz Rayleigh-Transport (KHRT) models are more appropriate for simulation of the ligament break-up regime, at We_g above 80.

Typically, within industry the outcome of the gas atomisation process is gov-

85 erned by operator skill and experience, with tweaks made and issues identified from the resulting impact on the powder produced. Over the years, research has attempted to develop robust simulation approaches, including a large amount of work which has focussed solely on the simulation of the gas flow-field generated by the atomising jets [13, 10, 14, 6, 16]. Ting and Anderson [12] used CFD

90 to investigate the atomising argon gas jet, focussing upon the phenomenon of "wake closure". Mi et al [6] also utilised CFD to simulate the effect of nozzle geometry on the structure of the supersonic jet formed, and pressures generated at the melt nozzle's exit.

Additionally, work has been undertaken to simulate the interaction between

95 the atomising gas jets and the melt. Pre-2005, the main focus of research work was upon primary break-up effects [10]; but, in more recent years, the simulation of secondary break-up has garnered further interest [5, 17, 15]. Simulating the mixing or interaction between compressible gas flow and weakly compressible liquid flow is an extremely complex simulation, due to the significant difference

100 in stiffness of gas and liquid metal [18]. The most advanced model available for its simulation being the volume of fluid (VOF). The VOF approach considers the gas and melt as immiscible, solving a single set of momentum equations, whilst tracking the respective volume fractions throughout the domain [19]. However, to implement this approach to capture a droplet accurately, would require at

105 least ten mesh divisions across the droplet's diameter; typically of the order of micrometres. Resulting in an excessively expensive simulation, beyond the capability of most readily available computational power [11].

Alternatively, a simulation between small droplets of molten liquid and gas is a more realistic simulation approach. Specifically, an Euler-Lagrange method,

110 which involves the fluid phase being treated as a continuum, modelled by solution of the Navier-Stokes equations (i.e. Eulerian); whilst, the dispersed phase is solved by tracking a large number of particles through the calculated flow-field. This approach can only be applied if the particles occupy a low volume fraction compared to the gas, i.e. less than 70% of the cell's volume before stability is-

115 sues become problematic [19]. Additionally, using two-way coupling allows the dispersed phase to exchange momentum, mass and energy with the fluid phase. However, in the majority of simulation work undertaken to-date, only one-way coupling has been employed; consequently the effect of the dispersed phase on the fluid is not considered [5].

120 Work at Greenwich University by Lena et al [20] utilised a fully coupled

4

Euler-Lagrange two-phase numerical scheme, with sub-models for particle break-up and phase-segregation. The droplet tracks, solidification history and inter-action with other droplets were modelled, in order to optimise the process and to predict defects.

125 Zeoli and Gu [21, 4, 15, 11] used a Euler-Lagrange model, with one-way coupling, to simulate the secondary droplet break-up and track the motion of the melt droplets within the flow-field. Firmansyah et al [5] undertook simulation work with the Euler-Lagrange configuration, using two-way coupling with Fluent's break-up models and compared their results to Zeoli's [11]. It was con-

130 cluded that their approach resulted in a more accurate representation of the gas atomisation process, due to the model's ability to capture the effect of the droplets on the flow and vice versa.

Generally however, an issue in developing an accurate simulation procedure is the validation of the model. The acquisition of detailed and accurate ex-

135 perimental data from the working environment of a gas atomiser is virtually impossible to attain due to the extreme operating conditions. Additionally, utilising the geometry of an actual industrial gas atomiser has issues due to safeguarding intellectual property.

Subsequently, it has been the intention to develop a simulation procedure

140 for an operational gas atomisation process which can be used as a predictive tool to assess the effect of process parameters on the PSD of atomised powders, using company supplied geometry and data (with all values normalised before being presented). A simulation tool of this type has the potential to provide huge benefit to atomised powder manufacturers, allowing them to exert better

145 control over the PSD of any powders produced; both the average particle size and standard deviation. Typically, as powder has to be supplied with tailored distributions to meet the requirements of its intended use e.g. ALM, any powder which falls outside requirements has to be re-melted and is classified as "reverb" [10]. It is essential to minimise this off-size powder inventory or reverb, to

150 ensure a powder producer remains competitive. A reduction in reverb having an obvious associated beneficial impact on overheads per process run and profit.

2. Modelling the fluid

Fluid flow is governed by the Navier-Stokes equations which are based upon three fundamental laws; which state that mass, momentum and energy must

155 all be conserved. The random nature of turbulent flow requires that variables describing the flow be decomposed into a steady mean value with a fluctuating component superimposed upon it [22]. For example, the velocity would become:

$$u(t) = \bar{u} + u'(t) \tag{2}$$

with this formulation termed the Reynold's decomposition. In order to transform the Navier-Stokes equations so that small-scale turbulent fluctuations do

160 not have to be directly simulated, the previously described decomposition of

5

variables into a mean and fluctuating value is applied. This results in the formulation of the Reynolds Averaging Navier-Stokes (RANS) equations. The RANS equations for steady-state, compressible flow, in conservative form are as follows [22]:

165   the RANS Continuity equation

$$\frac{\partial(\rho\bar{u}_i)}{\partial x_i} = 0 \tag{3}$$

the RANS momentum equation

$$\frac{\partial(\rho\bar{u}_i\bar{u}_j)}{\partial x_j} = -\frac{\partial\bar{P}}{\partial x_i} + \frac{\partial}{\partial x_j}\left[\mu\left(\frac{\partial\bar{u}_i}{\partial x_j} + \frac{\partial\bar{u}_j}{\partial x_i} - \frac{2}{3}\delta{ij}\frac{\partial\bar{u}_k}{\partial x_k}\right)\right] + \frac{\partial}{\partial x_j}(-\rho\overline{u_i'u_j'}) \tag{4}$$

where, ρ denotes the fluid density, u_i the ith component of the velocity vector and $-\rho\overline{u_i'u_j'}$ is termed the Reynolds Stress tensor, $(\tau_{ij})_{Re}$. The RANS models can be classified depending on how the $(\tau_{ij})_{Re}$ is calculated; with the

170   most widely used approach being the Eddy Viscosity Model (EVM). The EVMs assume that the "stress" is proportional to the strain, where strain is equivalent to the velocity gradients. The only unknown that needs to be calculated for this approach is an effective turbulent viscosity μ_t, using the Boussinesq hypothesis [22]:

$$(\tau_{ij})_{Re} = -\rho\overline{u_i'u_j'} = \mu_t\left(\frac{\partial u_i}{\partial x_j} + \frac{\partial u_j}{\partial x_i}\right) - \frac{2}{3}\left(\rho k + \mu_t\frac{\partial u_i}{\partial x_i}\right)\delta_{ij} \tag{5}$$

175   where, k is the turbulent kinetic energy per unit mass. Examples of EVM turbulence models include the standard $k-\epsilon$ [19, 22], the standard $k-\omega$ [19, 23] and the $k-\omega$ shear stress transport (SST) [23].

3. The discrete particle model and break-up mechanisms

To simulate the melt's secondary break-up a DPM can be implemented, using

180   the Euler-Lagrange approach. Considering the motion of the particles, their trajectory is predicted by the integration of a force balance on each particle, that equates the particle's inertia with the forces which act upon it; written in the Lagrangian reference frame [19]:

$$\frac{du_{p,i}}{dt} = \frac{(u_i - u_{p,i})}{t_p} + \frac{g_i(\rho_p - \rho_g)}{\rho_p} + F_i \tag{6}$$

The particle relaxation time, t_p, is given by:

$$t_p = \frac{24}{C_D Re_p}\frac{d_p^2\rho_p}{18\mu_g} \tag{7}$$

185   and the particle Reynolds number, Re_p:

$$Re_p = \frac{\rho_g d_p|u_{p,i} - u_i|}{\mu_g} \tag{8}$$

6

In equations 6 to 8, the index i indicates the three coordinates of particle position and velocity components; u_i refers to the fluid phase velocity, whilst $u_{p,i}$ refers to the particle velocity. μ_g is the molecular viscosity of the gas, ρ_g the density of the gas and ρ_p the density of the particle. d_p is the particle diameter, C_D the drag coefficient and the F_i term allows the incorporation of additional forces [19].

The dispersion of particles due to turbulence in the fluid phase can be predicted by using a stochastic tracking model, the "Discrete Random Walk" model; which includes the effect of instantaneous turbulent velocity fluctuations on the particles' trajectories [19].

In order to reproduce numerically the gas atomisation physics it is necessary to implement a model for the melt break-up. Three different break-up models have been considered in this work: the TAB model; the KH model; and the KHRT model. The TAB model is based upon the relationship between an oscillating and distorting droplet and a spring-mass system. The restoring force of the spring is represented by surface tension; whilst, the external force is substituted by aerodynamic forces. The liquid viscosity of the droplet is equitable to damping forces [11, 24]. The equation governing a damped forced oscillator is [19, 11, 24]:

$$f - Q\delta_{eq} - \Upsilon\frac{d\delta_{eq}}{dt} = m\frac{d^2\delta_{eq}}{dt^2} \tag{9}$$

Where, δ_{eq} is the displacement of the droplet equator from its spherical (undisturbed) position. From Taylor's analogy, the constants in Equation 9 can be defined as [19, 11, 24]:

$$\frac{f}{m} = C_f\frac{\rho_g u_{r,p}^2}{\rho_l r_p} \tag{10}$$

$$\frac{Q}{m} = C_Q\frac{\sigma}{\rho_l r_p^3} \tag{11}$$

$$\frac{\Upsilon}{m} = C_\Upsilon\frac{\mu_l}{\rho_l r_p^2} \tag{12}$$

Where, ρ_l and ρ_g are the discrete phase and continuous phase densities, $u_{r,p}$ is the relative velocity of the droplet, r_p the undisturbed droplet's radius. σ is the droplet surface tension and μ_l the droplet viscosity. C_f, C_Q and C_Υ are all constants determined from experimental and theoretical results, with values of 0.333, 8, and 5, respectively [24]. The "parent" droplet is assumed to break up into "child" droplets if the distortion grows to a critical ratio of the parent droplet's radius [19, 11, 24]: $\delta_{eq} > C_B r_p$, where C_B is a constant of value 0.5. To predict the child droplet sizes after break-up, the Sauter mean radius (SMR), $(r_p)_{32}$, of the droplet size distribution is assumed to be of the form [24]:

$$\frac{r_p}{(r_p)_{32}} = D_0 + D_1\left(\left(\frac{d\delta_{eq}}{dt}\right).\left(\frac{1}{C_B r_p \omega_n}\right)\right)^n \tag{13}$$

where, D_0, D_1 and n are all model constants found from experimental correlations to be 2.333, 3.0 and 0.5, respectively. [24].

7

Alternatively, the KH break-up model considers the break-up to be induced by the relative velocity between the gas and liquid phases. The model assumes that the time of break-up and the resulting droplet size are related to the fastest growing KH instability, derived from "Jet Stability" analysis [19]. The KH instability causes child droplets to be stripped from the liquid core of the jet, which is approximated by parent droplets which have the same radius R, as the injecting nozzle [25]. It is the wavelength and growth rate of the KH instability which are used to predict the details of the newly formed droplets. The wavelength of the instability is given by [19, 11, 25]:

$$\Lambda = \frac{9.02(1 + 0.45Z^{0.5})(1 + 0.4\Gamma^{0.7})}{(1 + 0.87We_g^{1.67})^{0.6}}R \tag{14}$$

Whilst, the growth rate of the wavelength is [19, 11, 25]:

$$\Omega = \frac{(0.34 + 0.38We_g^{1.5})}{(1 + Z)(1 + 1.4\Gamma^{0.6})}\left(\frac{\sigma}{\rho_l R^3}\right)^{0.5} \tag{15}$$

where, Z is the Ohnesorge number, a dimensionless value that relates the viscous forces to inertial and surface tension forces of the melt i.e. the Weber and Reynolds numbers, We_l and Re_l, respectively [25]:

$$Z = \frac{\sqrt{We_l}}{Re_l} = \nu\left(\frac{\rho_l}{\sigma R}\right) \tag{16}$$

where, ν is the kinematic viscosity of the melt.

Γ is the Taylor number, which relates Z to the gas Weber number, We_g [25]:

$$\Gamma = Z(\sqrt{We_g}) \tag{17}$$

The stable droplet's radius, r_s, resulting from atomisation is proportional to the wavelength of the fastest growing unstable surface wave:

$$r_s = B_0\Lambda \tag{18}$$

where, B_0 is a model constant of 0.61 [25]. Additionally, the growing KH instabilities govern the break-up time, t_B [19, 11, 25]:

$$t_B = \frac{3.7626B_1R}{\Lambda\Omega} \tag{19}$$

Where, B_1 is an adjustable model constant, that varies between $\sqrt{3}$ and 20 [25].

The KHRT model combines the effects of the KH model with the Rayleigh-Taylor (RT) instabilities due to acceleration of shed droplets ejected into free stream conditions [19]. Specifically, the child droplets shed from the liquid core of the jet, which exists in the near nozzle region, are subject to sudden acceleration when ejected into the free stream and a RT instability becomes the dominant effect [19].

As with the KH model the RT model describes the wave instabilities which form upon the droplet's surface; where, the frequency of the fastest growing wave is defined as:

$$\Omega_{RT} = \sqrt{\frac{2(-g_t(\rho_l - \rho_g))^{3/2}}{3\sqrt{3}\sigma(\rho_l + \rho_g)}} \tag{20}$$

where, g_t is the droplet acceleration in the direction of the droplet's travel. The wave number is given by:

$$W_{RT} = \sqrt{\frac{-g_t(\rho_l - \rho_g)}{3\sigma}} \tag{21}$$

break-up occurs after the RT waves have been growing for a time larger than the break-up time $(t_B)_{RT}$:

$$(t_B)_{RT} = \frac{1}{\Omega_{RT}} \tag{22}$$

the size of the new child droplets are dependent upon the RT wavelength, λ_{RT}:

$$\lambda_{RT} = \frac{2\pi}{W_{RT}} \tag{23}$$

with break-up only allowed when λ_{RT} is less than the diameter of the parent droplet. The number of new droplets is determined as the ratio of the maximum diameter of the deformed parent droplet to λ_{RT} and the corresponding diameter of the child droplets is obtained from mass-conservation principles [26].

The RT and KH models are implemented in a competing manner i.e. the droplet breaks up by the mechanism which predicts the shortest break-up time. Typically, in the regions closest to the injector nozzle, where the droplet velocities are highest, RT instabilities are the governing mechanism; whereas, the KH break-up becomes more dominant further downstream [26].

4. Process data

To facilitate the development of a simulation tool that would assess the impact of operational parameter changes on the PSD of powders produced by a close-coupled gas atomiser, data from LSN Diffusion Ltd., from approximately 1,500 atomiser process runs was provided. For all alloys, operating pressures (over a range of 1.50 MPa to 2.07 MPa), and melt flow-rates. The melt flow-rates have been normalised and considered in the range of 3 to 9. PSD data was provided from each of the process runs and from this a normalised average mean particle size (AMPS), along with the associated standard deviation was calculated for each run. A pan proportion which consists of powders which fall below the minimum powder size of saleable product was always removed from each process batch without undergoing sieving, being re-melted and used in subsequent process runs. The pan could typically account for between 30 to 40% of the powders produced from a batch. Subsequently, the normalised AMPS values have been calculated from provided process data with the pan

9

proportion removed - which actually accounts for a considerable percentage of
the powders produced during the secondary break-up process. Therefore, as part
of this study an attempt has also been made to assess the impact of including
the finer pan powder on the AMPS [27].

5. The computational model

Using the commercially available Fluent v14.5 software [28], a steady-state,
3D CFD simulation of a gas atomiser was undertaken. An axi-symmetric, ide-
alised nozzle configuration was implemented to reduce computational expense.
The geometry was provided by the powder manufacturing company LSN Diffu-
sion Ltd. Figure 2 illustrates the simulated geometry, for which the dimensions
have been normalised by a characteristic length L to protect the company's de-
sign. The computational domain considered, also normalised by L, extends 55.6
from the melt nozzle exit downstream and is 27.8 wide. It should be noted that
a range of different protrusion lengths were assessed as part of the investigation.

Figure 2: The simulated axi-symmetric geometry of the company's gas atomiser nozzle, with
normalised dimensions, using characteristic length L.

10

Fluent utilises a cell-centred finite volume method, with the Navier-Stokes governing equations discretised by a second order upwind scheme using a coupled-implicit density-based solver. An assessment was made between the standard $k - \epsilon$ and $k - \omega$ SST turbulence models. The former being commonly used in previous simulation studies of the gas atomisation process [12, 6]; whilst, the latter is recommended for the accurate simulation of shock waves [29]. Subsequently, the $k - \omega$ SST was selected and utilised based on comparison of initial simulation results, where it was found to produce sharper approximations of the shock waves as compared to more smeared or averaged results captured by the standard $k - \epsilon$ simulation [27].

Using Fluent's material database, nitrogen was selected for the simulated gas; with the "Ideal Gas" formulation used in place of density as the flow was anticipated to be compressible. The boundary conditions are labelled in Figure 3; where, the gas to the inlet was supplied at a range of different values as part of an assessment of the effect of operating pressure on powder production; and the pressure outlet maintained at atmospheric.

Figure 3: An overview of the boundary conditions used for the simulation of the gas atomiser.

In order to approximate the PSD of powder produced by the modelled gas atomiser, a simulation of the secondary break-up phase was considered. A transient, two-way coupled Euler-Lagrange DPM was utilised. The transient simulation was started from the converged steady-state gas-only simulation and run with a time-step of 10^{-6} s, using the DPM model available within Fluent. Droplets of diameter 1 mm were injected at the melt nozzle outlet's top corner, at a temperature of 1873.15 K. To approximate the alloy powders manufactured, a metal with the following physical properties: density $7700 kg/m^3$; specific heat capacity 723 J/kg K; viscosity 0.0056 kg/m s; and surface tension in the range of 1.2 N/m to 1.8 N/m [4, 30]. A range of different melt flow-rates were considered, for comparison with the process data provided.

Two different approaches for simulation of the break-up mechanisms were considered and subsequently compared: first, the method developed by Zeoli [4] was integrated into Fluent's DPM model by user defined function (UDF), which uses both the KH and TAB model, with a transition between the two at a We_g of 80; second, utilised the KHRT model within Fluent's DPM.

6. Results and discussion

Mesh sensitivity and convergence. A full convergence and mesh sensitivity study was undertaken; considering a generic mesh spacing of δ, meshes in the range of 2δ to $2\delta/5$ were produced. Convergence of the steady-state fluid-only atomising gas jet simulation was assessed from comparing the average value of aspiration pressure after a substantial increase in the number of iterations; with aspiration pressure utilised due to its effect on the efficiency of the gas atomisation process.

11

Provided that the values differed by no more than 5% then the simulation was deemed converged.

Considering the effect of mesh size, it was observed that the difference between the converged aspiration pressure values for the finest mesh considered i.e. $2\delta/5$ mesh spacing, and the other coarser meshes was well below 5% for a mesh spacing of δ or finer, as illustrated by Figure 4. Ideally, for increased accuracy of the fluid only CFD simulation (with limited computational expense penalty) a finer mesh with spacing of $\delta/2$ i.e.130,000 elements could be utilised. However, it was established that in order to achieve a converged result from the DPM at high particle loadings, it was necessary to use a mesh with element dimension size of δ i.e. 33,000 elements. This was to ensure that the 70% maximum discrete phase occupation (a restriction of the Euler-Lagrange DPM method) wasn't exceeded, which would cause the simulation to diverge.

Figure 4: A plot of the effect of mesh size on the average aspiration pressure

Figure 5 shows the results of the convergence study undertaken for the KHRT model, which shows that approximately 7 ms of simulation time was required for the AMPS values produced to reach a settled value. The Zeoli KH-TAB model was found to have reached a converged particle size in the time-frame required for the particles to reach the end of the domain; typically around 1.5 ms.

Figure 5: Demonstrates the time taken to reach a converged normalised average mean particle size (AMPS) when utilising the KHRT break-up model.

Atomising gas jet CFD results. Figure 6 provides an overview of the initial fluid structure established in the region adjacent to the nozzle exit prior to the introduction of the melt. Distinct flow features have been identified and labelled, typical of the flow-field at the rear shoulder of a blunt based body and in under-expanded jet flow. A clear Mach disc, closed-wake condition is observed, along with the subsequent circulating region created under the melt nozzle exit. More detailed results and analysis from the CFD simulation of the atomising gas jets can be found in work by Thompson [27].

Figure 6: Velocity contours developed in the region adjacent to the atomising jet's nozzle exit, prior to the introduction of the melt; several distinct flow features associated with under-expanded jet, rear shoulder blunt based body flow are labelled

12

Melt break-up simulation and validation. Figure 7 shows the particle trajectories produced for the KH-TAB and the KHRT break-up models, respectively. It is
360 clear from the simulations that the latter has produced a comet-like cloud of disintegrating molten metal particles with the smallest particles produced of the order 10^{-9} m. This is in stark contrast to the KH-TAB approach, which has resulted in a narrow track of particles that is gradually drawn down onto the central axis, exhibiting less extensive break-up of the droplets; the smallest
365 droplet diameter being of the order 10^{-4} m. This was also noted in previous research [5], and is attributable to the unsteady feature of droplet streaming being neglected.

Figure 7: The particle trajectories for Zeoli's KH-TAB (left image) and Fluent's KHRT (right image) secondary break-up models

Figure 8 and Figure 9 present the particle diameter and temperature data extracted from Fluent for the particle trajectories for the KH-TAB and the
370 KHRT break-up models, respectively. A greater range in particle sizes is noted for the KHRT model, that is split into a group of parent droplets gradually decreasing in size and the considerably smaller child droplets generated. The large range of sizes has resulted in a much larger spread of particle droplet temperatures, due to the effect that size has on cooling rate. A gradual decrease
375 in both particle diameter and temperature is exhibited for the KH-TAB model, with a clear discontinuity observed close to 1 ms, that coincides with a We_g of 80 and the switch from the KH to the TAB model.

Figure 8: Droplet diameter and temperature history for the Zeoli KH-TAB break-up model

Figure 9: Droplet diameter and temperature history for the KHRT break-up model

14

An assessment was made as to the impact of the particles on the atomising gas jet's flow. Figure 10 provides a graphical overview of the effect of the particle loading on the stream-wise velocity. From which it is clearly evident that the particle loading of the KHRT model has had a greater impact on the fluid flow's behaviour, as compared to the KH-TAB model. The energy of the atomising jet is obviously diminished by the heavier particle loading of the KHRT model, with the stream-wise velocity reducing quite dramatically at a normalised (by L) distance of 11 from the melt nozzle's exit and further downstream. Considering the effect of the KH-TAB model, there are changes in the atomising jet's behaviour, but it has retained many of the same features as the unloaded atomising jet, with the same oscillations in velocity attributable to its under-expanded jet structure. Figure 11 shows the velocity contours generated for the gas only flow compared to the gas flow for the converged DPM simulations of the KHRT model, which further illustrates the effect of the relatively dense particle loading upon the gas flow. Specifically, the maximum velocity has reduced by approximately 3%; the length of the first circulating region has been reduced; the second circulating region is slightly enlarged; and, the velocity downstream of the second circulating region has been reduced, with the jet opening out and not reflecting back onto the centreline as strongly (i.e. the strength of the under-expanded jet has diminished). These results emphasise the importance of utilising the two-way coupling when simulating the gas atomiser with a realistic heavy particle loading (i.e. as generated from the Fluent KHRT break-up model). It also explains the time required for the simulation to achieve a converged AMPS result; with, the iterative process between the particles effecting the flow-field and vice-versa, taking time to settle.

Figure 10: A graph illustrating the effect of particle loading from the KH-TAB and the KHRT models on the Stream-wise velocity when simulating at a process melt flow-rate of 9

Figure 11: A comparison of the velocity contours generated without (top) and with (bottom) particles for the Fluent KHRT break-up model

15

Fluent's KHRT and Zeoli's KH-TAB break-up models were compared for different melt flow-rates (i.e. where increasing melt flow-rate corresponds to decreasing gas-to-melt ratio (GMR) value). Figure 12 provides a graphical overview of a comparison between the simulation results and the process normalised AMPS data, including standard deviation. It can be seen that the process data's trend of increasing AMPS with increasing melt flow-rate (decreasing GMR) has been produced by the Fluent KHRT model. The KH-TAB model however, has produced the inverse relationship, with AMPS decreasing with increasing melt flow-rate. Considering the quantitative predictive ability of the models, on reviewing Figure 12, it is evident that the KH-TAB model has widely over-estimated the normalised AMPS values. The KHRT model has under-predicted as compared to the process data presented without the pan proportion. However, has reasonably estimated the normalised AMPS value of the process data with an approximation of the pan data included. Therefore, there is potential for the KHRT model to demonstrate quantitative estimating ability, although this must be verified by attaining a complete PSD of powder produced including pan proportion.

Figure 12: The effect of normalised melt flow-rate on normalised AMPS for the process data both with and without the pan proportion, compared to Zeoli's KH-TAB and Fluent's KHRT break-up models

To assess the effect of operating pressure, protrusion length and surface tension, the KHRT break-up model has been used, after being identified as a more realistic simulation approach than the KH-TAB model.

Effect of operating pressure. Figure 13 illustrates the effect of operating pressure on the normalised AMPS process data and the KHRT model simulation results at a melt flow-rate of (approximately if considering the process data) 5. From this, a similar trend can be identified for both the simulation and process data of increasing pressure resulting in decreasing AMPS; with the simulation again tending to under predict the AMPS values as compared to the process data (without pan).

Figure 13: A graph illustrating the effect of operating pressure on normalised AMPS at a normalised melt flow-rate of 5 for both the process data (without pan) and the KHRT break-up model simulation

16

₄₃₀ *Effect of protrusion length.* The model was used to predict the effect of normalised protrusion length on the AMPS of powder size produced; additionally, an estimate of the industry-specific criterion of d_{84}/d_{50} has been calculated [5]. This is used as a measure of the width of particle size distribution i.e. comparable to a measure of standard deviation. Figure 14 shows the effect of
₄₃₅ normalised melt nozzle protrusion length on the normalised AMPS as predicted by the simulation at a normalised melt flow rate of 5; where it can be seen that as protrusion length increases so does the AMPS. Figure 15 shows the mass-based cumulative size distribution for the simulation at the three normalised protrusion lengths of 0, 1.11 and 2.22. From this plot, values of d_{84}/d_{50} were
₄₄₀ calculated to be 1.32, 1.95 and 2.1, respectively; establishing the relationship that the standard deviation increases with increasing protrusion length.

Figure 14: A graph illustrating the effect of normalised protrusion length on normalised AMPS at a normalised melt flow-rate of 5 for the KHRT break-up model simulation

Figure 15: Mass-based cumulative size distribution plots for increasing normalised protrusion lengths from Fluent's KHRT break-up model data at a normalised melt flow-rate of 5

17

Effect of melt surface tension. Utilising the predictive ability of the model, the effect of melt surface tension on the normalised AMPS, at a normalised melt flow-rate of 5 was assessed. From Figure 16 it can be seen that the simulation has predicted that increasing the σ results in increasing the AMPS. From Figure 17, d_{84}/d_{50} values could be predicted of 2.1, 1.9 and 1.8 for the σ values of 1.2, 1.6 and 1.8 N/m, respectively; showing that, as σ increases the standard deviation decreases.

Figure 16: A graph illustrating the effect of melt surface tension (σ) on normalised AMPS at a normalised melt flow-rate of 5 for the KHRT break-up model simulation

Figure 17: The mass-based cumulative size distribution plots for melt surface tension (σ) from Fluent's KHRT break-up model data at a normalised melt flow-rate of 5

18

Discussion. Utilising the process data the relationship between the melt flow-rate and AMPS has been established and used to identify and validate the KHRT break-up model as an accurate simulation approach of the close-coupled gas atomiser considered. The general trend established of increasing AMPS with increasing melt flow-rate can be attributed to the increased melt flow loading in the core of the atomising jets causing a reduction in the effective supersonic region. Subsequently, this has a limiting effect on the secondary break-up, resulting in coarser powder production.

Additionally using the KHRT break-up model, it was established and validated that increasing operating pressure results in the production of finer powders. This is caused by the increasing operating pressure resulting in the elongation of the supersonic region of the gas jet and the subsequent extension of secondary break-up.

Based on confidence established from the validated model results regarding the effect of operating pressure and melt flow-rate, the KHRT break-up model was used to predict the effect of both protrusion length and melt surface tension on the PSD of powders produced from the company's process. It was established that as the melt nozzle's protrusion length is decreased, finer powders are produced. Considering the atomisation process, there is less negative draw at the melt exit, as compared to longer protrusion lengths; but, there is improved radial draw of the melt into the atomising jets, which improves the efficiency of break-up resulting in finer powder production with a smaller standard deviation.

The simulation predicted that increasing surface tension will result in larger particle sizes with a narrower range of sizes. This outcome should be expected, as surface tension is increased, more energy is required to be transferred to the particles to promote break-up. As the surface tension is increased the break-up process becomes less efficient, with generally fewer particles breaking down and the outcome being larger particles with less of a deviation in size.

7. Conclusions

The development of a robust simulation tool that could be used for the prediction of the effect on PSD of powder produced by an operational gas atomiser was investigated. By utilising an Euler-Lagrange approach, a simulation of the interaction between the atomising gas jets and the molten droplets could be assessed. Focussing upon the secondary break-up phase of the atomisation process allowed for the comparison between two different break-up models. One, the Fluent in-built KHRT model; and the second, a model developed by Zeoli [21] that utilises both the KH and TAB models, implemented into the Fluent software using a UDF. Using PSD data made available from the company permitted the identification of which model was most representative of the real-world process. Subsequently, the following conclusions have been drawn regarding the break-up model:

- It was clearly established that increasing the melt flow-rate (decreasing the GMR) results in an increase in the AMPS of the powders produced,

19

attributable to the increased melt loading in the core of the atomising jet, diminishing its effectiveness.

- The KHRT model produced a far more realistic particle track, generating a cloud of particles, as opposed to the steady, single stream produced by Zeoli's model; which did not appear to produce an appropriately randomised number of child particles from the parent droplets i.e. neglecting of the unsteady features of droplet streaming.

- The KHRT model accurately predicted the effect of melt flow-rate and showed potential to accurately predict the values, especially when considering the AMPS values calculated with an estimated pan proportion included.

- Zeoli's model greatly over-predicted the average particle size and inaccurately predicted the effect of melt flow-rate on particle size.

- Due to the heavier particle loading of the KHRT model, two-way coupling was essential to approximate the impact of the particles on the fluid flow's behaviour; the low particle loading of Zeoli's model illustrated that two-way coupling was not as critical.

- Subsequently, the KHRT model is identified as more accurate and robust for the simulation of the break-up process.

The validated KHRT model was then used to consider the effect of operating pressure, for which limited data was available for comparison; and, melt properties and nozzle geometry, for which no process data was available and the model's predictions had to be explained on consideration of the physics of the gas atomisation process. From this, further confidence was gained in the model's ability to predict the effect of operational parameters and geometry on the PSD of powders produced. Provision of further process data from the company, including a PSD which includes the pan proportion will allow for further refinement of the model. Generally, it was established that:

- Increasing operating pressure results in a decrease in particle size.

- Increasing protrusion length results in a decrease in particle size and the spread of the particle sizes produced.

- Increasing the melt surface tension results in an increase in particle size and a decrease in the spread of particle sizes produced.

- The simulation approach has proven itself to be useful as a predictive tool for the assessment of altering operational parameters and nozzle geometry on the PSD of powders produced.

- Further development of this tool will provide the company with a powerful aid in the continuing intention to optimise their gas atomisation process for the production of powders for ALM manufacturing.
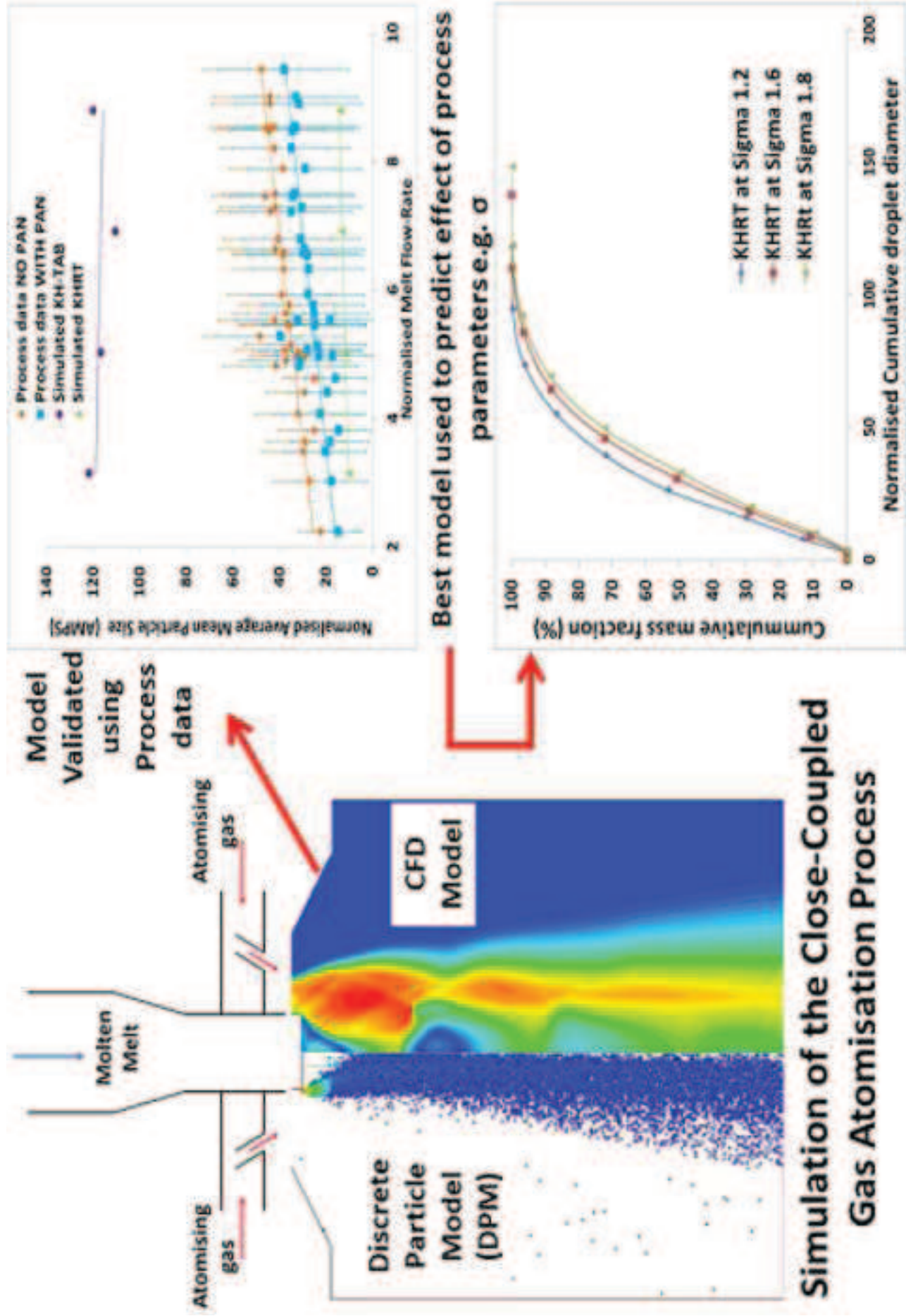
20

Acknowledgements

References

[1] A. Yule, J. Dunkley, Atomization of melts for powder production and spray deposition, Oxford University Press, USA, 1994.

[2] G. Antipas, Gas atomization of aluminium melts: Comparison of analytical models, Metals 2 (2) (2012) 202–210.

[3] I. Anderson, J. Ricken, J. Meyer, D. Byrd, A. Heidloff, Visualization of atomization gas flow and melt break-up effects in response to nozzle design variations: simulation and practice, in: Advances in Powder Metallurgy and Particulate Materials - 2011, Proceedings of the 2011 International Conference on Powder Metallurgy and Particulate Materials, PowderMet 2011; Part 2Particulate Production, MPIF, 2011, pp. 180–197.

[4] N. Zeoli, H. Tabbara, S. Gu, Cfd modeling of primary breakup during metal powder atomization, Chemical Engineering Science 66 (24) (2011) 6498 – 6504.

[5] D. Firmansyah, R. Kaiser, R. Zahaf, Z. Coker, T. Choi, D. Lee, Numerical simulations of supersonic gas atomization of liquid metal droplets, Japanese Journal of Applied Physics 53 (5S3) (2014) 05HA09.

[6] J. Mi, R. Figliola, I. Anderson, A numerical investigation of gas flow effects on high-pressure gas atomization due to melt tip geometry variation, Metallurgical and Materials Transactions B 28 (5) (1997) 935–941.

[7] C. Lea, Underexpanded jets, `http://uriah.dedi.melbourne.co.uk/w/index.php/Underexpanded_jet` (October 2013).

[8] B. Massey, J. Ward-Smith, Mechanics of Fluid 7th Edition, Stanley Thornes Ltd., Cheltenham, UK, 1998.

[9] J. Ting, M. Peretti, W. Eisen, The effect of wake-closure phenomenon on gas atomization performance, Materials Science and Engineering: A 326 (1) (2002) 110–121.

[10] S. Mates, G. Settles, A study of liquid metal atomization using close-coupled nozzles, part 1: Gas dynamic behavior, Atomization and Sprays 15 (1).

[11] N. Zeoli, Multiphase modelling of the characteristics of close coupled gas atomization, Ph.D. thesis, Aston University (2011).

21

[12] J. Ting, I. Anderson, A computational fluid dynamics (cfd) investigation of the wake closure phenomenon, Materials Science and Engineering: A 379 (1) (2004) 264–276.

[13] O. Aydin, R. Unal, Experimental and numerical modeling of the gas atomization nozzle for gas flow behavior, Computers & Fluids 42 (1) (2011) 37 – 43.

[14] M. Tong, D. Browne, Modelling compressible gas flow near the nozzle of a gas atomiser using a new unified model, Computers & Fluids 38 (6) (2009) 1183–1190.

[15] N. Zeoli, S. Gu, S. Kamnis, Numerical modelling of metal droplet cooling and solidification, International Journal of Heat and Mass Transfer 51 (15) (2008) 4121–4131.

[16] A. Allimant, M. Planche, Y. Bailly, L. Dembinski, C. Coddet, Progress in gas atomization of liquid metals by means of a de laval nozzle, Powder Technology 190 (1) (2009) 79–83.

[17] D. Bergmann, U. Fritsching, K. Bauckhage, A mathematical model for cooling and rapid solidification of molten metal droplets, International journal of thermal sciences 39 (1) (2000) 53–62.

[18] J. Caltagirone, S. Vincent, C. Caruyer, A multiphase compressible model for the simulation of multiphase flows, Computers & Fluids 50 (1) (2011) 24–34.

[19] A. Fluent, Ansys fluent theory guide v14.0 (2012).

[20] C. Lena, G. Djambazov, K. Pericleous, et al., Modelling metal powder production by the gas atomisation process, The Minerals Metals and Materials Society, 2008.

[21] N. Zeoli, S. Gu, Computational simulation of metal droplet break-up, cooling and solidification during gas atomisation, Computational Materials Science 43 (2) (2008) 268–278.

[22] H. Versteeg, W. Malalasekera, An introduction to computational fluid dynamics: the finite volume method, Pearson Education, 2007.

[23] A. Bakker, Applied turbulence modelling - lecture 10 turbulence models, http://www.bakker.org/dartmouth06/engs150/10-rans.pdf (July 2012).

[24] Chapter 5: Dispersed phase closure models, http://www.tfd.chalmers.se/ valeri/book-chapt5.pdf (February 2014).

[25] M. Turner, S. Sazhin, J. Healey, C. Crua, S. Martynov, A breakup model for transient diesel fuel sprays, Fuel 97 (2012) 288–305.

22

[26] G. Stiesch, Modeling engine spray and combustion processes, Springer Science & Business Media, 2013.

[27] J. Thompson, The development of simulation procedures for industrial mixing processes, Ph.D. thesis, Swansea University (2015).

610 [28] A. Fluent, Fluent user guide v14.0 (2012).

[29] Y. Bartosiewicz, Z. Aidoun, P. Desevaux, Y. Mercadier, Numerical and experimental investigations on supersonic ejectors, International Journal of Heat and Fluid Flow 26 (1) (2005) 56–70.

[30] C. Costa, S. Delsante, G. Borzone, D. Zivkovic, R. Novakovic, Thermo-615 dynamic and surface properties of liquid co–cr–ni alloys, The Journal of Chemical Thermodynamics 69 (2014) 73–84.

23

Graphical Abstract

Model Validated using Process data

Best model used to predict effect of process parameters e.g. σ

Discrete Particle Model (DPM)

CFD Model

Atomising gas

Molten Melt

Atomising gas

Simulation of the Close-Coupled Gas Atomisation Process

Highlights for "The identification of an accurate simulation approach to predict the effect of operational parameters on the Particle Size Distribution (PSD) of powders produced by an industrial close-coupled gas atomiser"

- A comparison of models to simulate gas atomisation secondary break-up is presented.
- The validated model combines CFD and a discrete particle model with KHRT break-up.
- The model has been used to predict the effect of parameters on atomised powder PSD.
- Results indicate potential for a predictive model used to optimise powder production.